case, the background signal is the radiance arising from diurnal surface heating, integrated over the spacecraft-facing hemisphere. Although thermal data are available from Voyager 1 for various portions of the surface, a comprehensive surface temperature model is not yet complete. A conservative estimate of the ability to detect thermal anomalies can be made, however; viewed at emission angle θ, a circular source should be detectable at, say, 650 cm^{-1} if

$$R^2B(T) \cos \theta \geq 0.08$$

where R is the source radius (in kilometers) and $B(T)$ is the Planck function (W cm^{-2} sr^{-1}/cm^{-1}) at temperature T (in degrees kelvin). Thus a thermal event of the magnitude observed by Witteborn *et al.* (*3*), which could be interpreted as an area 52 km in radius at 600 K, would have been observable from the spacecraft if present on the satellite at a view angle of less than 70°. An area 100 km in radius at 290 K, such as that observed from Voyager 1 (*1*), would have been observable if at a view angle less than 54°. That no such anomalies were seen limits the thermal emission from the source of plume 8 (*5*), which was near an emission angle of 45° during the Voyager 2 observations. For example, an exposed area of molten sulfur (385 K) could be no more than 50 km in radius. Further analysis will refine the detection limit and will also enable limits to be placed on the activity associated with plumes 2 and 5, which were very near the limb at this time.

The flyby of Europa provided IRIS spatial resolution of only about one-third of the disk. Limited coverage (15 to 21 hours local time) of the diurnal thermal cycle of the surface was therefore obtained. Surface temperatures between 0° and −40° latitude ranged between 85 and 110 K. This range is consistent with a diurnal maximum equatorial temperature of ~ 125 K.

Although covering a different hemisphere, the Voyager 2 flyby of Ganymede observed a range of local times similar to that obtained during the Voyager 1 flyby (11 to 24 hours local time). Surface temperatures at low latitudes ranged between 85 and 145 K. A slight wave-number dependence of brightness temperature (approximately 5 K higher at 600 cm^{-1} than at 250 cm^{-1}) is observed. This is generally consistent with the presence of a range of surface temperatures within the instrument field of view, as might be caused by variations in surface albedo and thermal inertia.

The Voyager 2 flyby of Callisto provided the only dawn terminator coverage

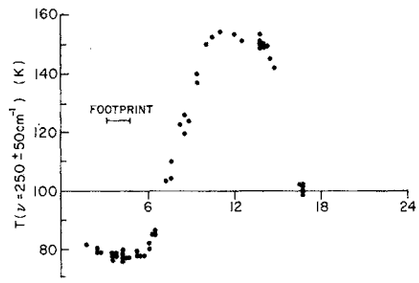

Fig. 7. Brightness temperatures at 250 cm^{-1} versus local time for Callisto. Prenoon data are from Voyager 2; afternoon data are from Voyager 1. Measurements were taken from latitudes between −10° and +25°. The approximate range of local time covered by the instrument footprint is indicated. Pointing uncertainties of ± 1 hour in local time may exist.

of a satellite. A plot of low-latitude brightness temperatures at 250 cm^{-1} is shown in Fig. 7. The predawn cooling portion of the curve can be used to estimate the thermal inertia of the near surface layers. According to a heat conduction model with physical properties independent of depth, diurnal heating calculations imply a value of $\sim 2 \times 10^{-3}$ cal cm^{-2} K^{-1} $sec^{-1/2}$. This is about twice as high as the value for Earth's moon obtained under similar assumptions. The comparison suggests that Callisto has a more consolidated subsurface than has Earth's moon, as might be expected if refusion of icy material occurs. The assumption of vertically homogeneous properties is actually invalid; eclipse observations of Callisto indicate a surface layer approximately 1 mm thick with a thermal inertia of $\sim 2 \times 10^{-4}$ cal cm^{-2} K^{-1} $sec^{-1/2}$ overlying a higher inertia layer (*6*). The present result is consistent with this. Not surprisingly, the daytime behavior of the surface temperatures in Fig. 7 is not well described by the homogeneous model. While the morning warming behavior can be fit with such a model, the afternoon cooling is too rapid. An additional complication is also introduced by a variation in the wavenumber dependence of the brightness temperature with local time. Preliminary attempts to model this behavior with two surface components of different albedos have not been successful. More sophisticated modeling is under way.

R. HANEL, B. CONRATH
M. FLASAR, L. HERATH
V. KUNDE, P. LOWMAN
W. MAGUIRE, J. PEARL
J. PIRRAGLIA, R. SAMUELSON
Goddard Space Flight Center, Greenbelt, Maryland 20771
D. GAUTIER
Paris Observatory, Meudon, France
P. GIERASCH
Cornell University, Ithaca, New York 14853
L. HORN, S. KUMAR
Jet Propulsion Laboratory, Pasadena, California 91103
C. PONNAMPERUMA
University of Maryland, College Park 20742

References and Notes

1. R. Hanel *et al.*, *Science* **204**, 972 (1979).
2. B. A. Smith *et al.*, *ibid.*, p. 951.
3. F. C. Witteborn, J. D. Bregman, J. B. Pollack, *ibid.* **203**, 643 (1979).
4. B. A. Smith *et al.*, *ibid.* **206**, 927 (1979).
5. R. G. Strom, R. J. Terrile, H. Masursky, C. Hansen, *Nature (London)*, in press.
6. D. Morrison and D. P. Cruikshank, *Icarus* **18**, 224 (1973).

7. We thank D. Vanous, D. Crosby, and J. Taylor and their colleagues at Texas Instruments, Goddard Space Flight Center, and Jet Propulsion Laboratory (JPL) for preparation of the instrumentation. F. Rockwell, C. Otis, J. Frost, and P. Corbin (Astro Data Systems, Inc.) contributed substantially to the data reduction. T. Burke, E. Miner, and D. Collins (JPL) made substantial contributions. We also thank the imaging team, especially B. Smith, G. Hunt, and R. Terrile for many discussions and for help in the selection of 5-μm "hot spots" for IRIS observations. The support of the Voyager Project staff is also gratefully acknowledged. Portions of the research described in this report were supported by JPL, California Institute of Technology, under NASA contract NAS 7-100.

27 September 1979

Photometric Observations of Jupiter at 2400 Angstroms

Abstract. *The photopolarimeter instrument on Voyager 2 was used to obtain a map of Jupiter at an effective wavelength of 2400 angstroms. Analysis of a typical north-south swath used to make this map shows strong absorption at high latitudes by a molecular or particulate constituent in the Jovian atmosphere. At 65° north latitude, the absorbing constituent extends to altitudes above the 50-millibar pressure level.*

During the approach phase of the Voyager 2 encounter with Jupiter, the photopolarimeter instrument (*1*) was programmed to obtain intensity measurements every 0.6 second by using a 300-Å bandpass filter centered at 2350 Å. When convolved with the solar flux, the effective wavelength of these observations is 2400 Å. With the spacecraft a nominal 48 Jupiter radii (R_J) from Jupiter, the subspacecraft point at 4.5° north latitude, the phase angle 17.5°, and the subsolar point at 0° latitude, the scan-platform pointing direction was articulated

0036-8075/79/1123-0956$00.50/0 Copyright © 1979 AAAS

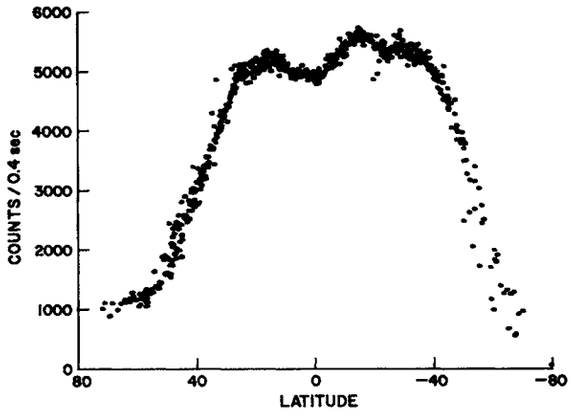

Fig. 1. Photon counts plotted against planetary latitude at 2400 Å. Data from 48 north-to-south scans along Jupiter's central meridian are plotted.

from north to south in 48 successive swaths covering a 10-hour period (one complete rotation of Jupiter). Each north-south swath consisted, alternately, of 16 or 13 discrete pointings spaced along the subspacecraft meridian; data were obtained for 48 seconds at each pointing. The photopolarimeter instrument used a 0.07° field of view, yielding a spot size of 1/16 R_J. Figure 1 shows an ensemble of 690 measurements, with count rate per 0.4 second plotted as a function of latitude. (Four missing swaths were filled by using data from the previous rotation of the planet.) A very consistent pattern for successive swaths is shown, with the equatorial region depressed in intensity. The brightest intensities occur at 15° south latitude.

Figure 2 shows a false color map of Jupiter at 2400 Å. The color scale was made by squaring the intensity (count rate) and using 16 colors from bright yellow to dark blue, in order of decreasing intensity. The latitude-longitude scale is a cylindrical projection of Jupiter; the longitude scale is system III, with the Great Red Spot (GRS) appearing at 109° longitude. The map has been smoothed to fill in data gaps.

The north-south scan data present an immediate surprise in terms of the amount of structure present at 2400 Å. The GRS at the resolution of our north-south map is ~15 percent darker than the South Temperate Zone (STeZ); the South Equatorial Belt (South) (SEB_s) is ~15 percent brighter than the equatorial region. Thus the absorption features of the various cloud species continue into the ultraviolet (UV) [although not always in the same sense as at visible wavelengths; at 2400 Å the SEB_s is the brightest feature on Jupiter, brighter even than the North Tropical Zone (NTrZ)]. Furthermore, the absorbing materials are located high enough in the atmosphere so that bright Rayleigh scattering from overlying gas does not obscure these contrasts.

The altitude of absorbers that are responsible for the banded structure in the UV has not yet been determined. However, if the contrasts are produced by aerosols in the visible clouds near 0.6 bar, our data place severe constraints on aerosol single-scattering albedos ($\tilde{\omega}$) at this level. For example, the contrast between the STeZ and the GRS would require very absorptive ($\tilde{\omega} \leq 0.84$) particles in the GRS, if the zone aerosols have $\tilde{\omega} = 0.994$. Furthermore, as shown below, additional absorption at higher altitudes is required by Jupiter's low geometric albedo.

A second surprise is the very strong absorption at high latitudes. North of 30° north, and south of 50° south, the intensity decreases much more rapidly than for a Lambert sphere; at 60° north in the North Polar Region (NPR), Jupiter is only half as bright as predicted by a Lambert reflector normalized to mid-latitudes. The remarkable darkness at 2400 Å of the NPR and the South Polar Region (SPR) has to be reconciled with the high efficiency of conservative Rayleigh scattering at this wavelength. We present several models to bound the multidimensional range of possibilities.

The north-south scan data can be fitted by many kinds of models, given sufficient free parameters. We have experimented with a sequence of models of increasing complexity. First, simply choosing the proper value of the reflectivity of a Lambert surface for each data point provides such a fit, although without any physical importance. Second, and more significant, is a model of pure conservative (nonabsorbing) Rayleigh scattering by gas (of Jovian composition)

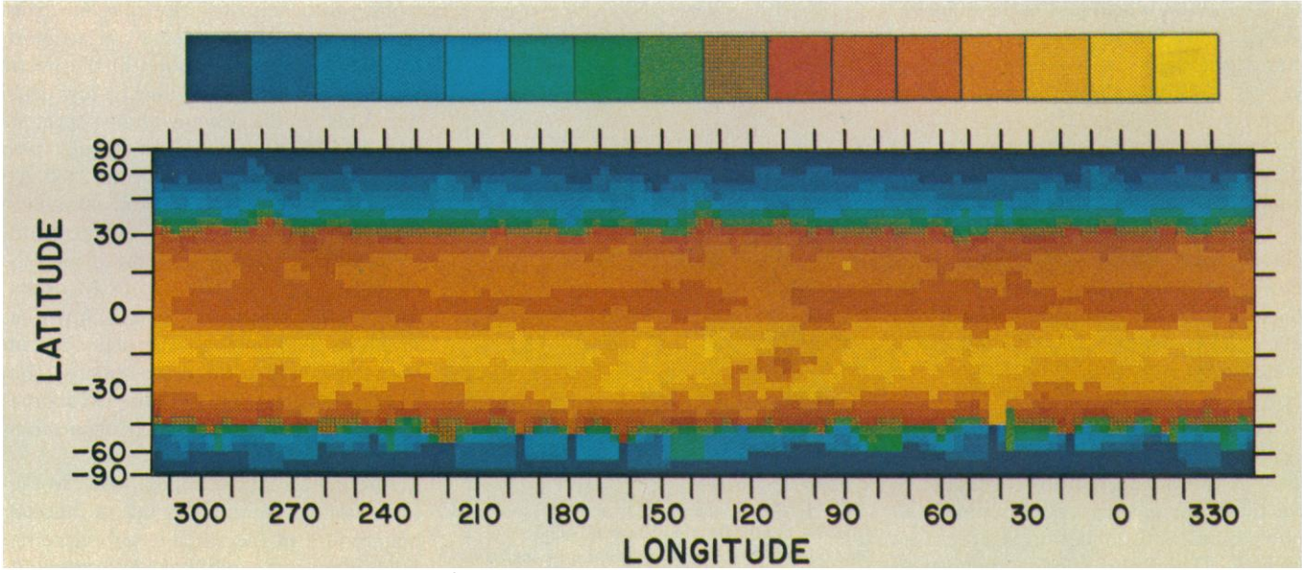

Fig. 2. Cylindrical projection of Jupiter at 2400 Å. The data were assembled from successive north-to-south scans along Jupiter's central meridian; the image covers 360° of longitude. The GRS (system III longitude, 109°; latitude, 23° south) can be seen as a dark feature near the center of the map.

above a black surface. Each data point is fitted exactly by adjusting the location of the surface. The implied pressure levels of the black surface are shown in Fig. 3. An immediate conclusion is that under no circumstances can there be more than 400 mbar of clean nonabsorbing gas over the mid-latitude regions; otherwise, these regions would appear brighter. This is based on our normalization of the north-south data scans to a geometric albedo of Jupiter of 0.30 at 2400 Å (*2*). There can be no more than 40 mbar of clean nonabsorbing gas over the NPR at 65° latitude. This is remarkable considering the evidence for enhanced Rayleigh scattering at high latitudes (*3*). The darkness of the NPR at 2400 Å implies that the absorbing material is very high (less than 40 mbar) and is sufficiently dark to eliminate reflection from the deeper atmosphere. In this model, the GRS is higher than the STeZ by 3.0 km.

Our north-south map data can also be explained by models having a semi-infinite homogeneous mixture of gas and black absorbing particles or molecules characterized by their optical concentration, τ_a/τ_R, where τ is optical depth, a is absorption, and R is Rayleigh scattering. The data points can all be fitted exactly by adjusting this concentration ratio from a minimum of 0.08 for the STeZ to a maximum of 1.3 for the NPR. For a given concentration, an equivalent pressure P_e can be defined, namely the pressure at which the total vertical optical depth $(\tau_a + \tau_R)$ equals unity. This is given by $P_e = 300/(1 + \tau_a/\tau_R)$ mbar and is shown in Fig. 3. The effective pressure varies only by a factor of 2 between the mid-latitudes (P_e = 260 mbar) and the NPR (P_e = 130 mbar), but the effective depth of penetration is still less in the polar regions. In this model, the altitude of optical depth unity in the GRS (with $\tau_a/\tau_R = 0.14$) is only slightly higher (0.7 km) than for the STeZ.

Observations of equivalent widths and center-to-limb variations of absorption bands have led previous investigators (*4*, *5*) to design models in which several cloud layers are used. To demonstrate the restrictions that our data place on these models, we calculated reflectivities using the model by Sato and Hansen (*5*), which is sketched in Fig. 4. Only the properties of this model at and above 650 mbar have any effect on intensity at 2400 Å. Particles (or molecules) absorbing at 2400 Å are mixed uniformly relative to the molecular gas from the bottom of the upper cloud at 650 mbar up to a pressure level P_0. The upper cloud, assumed to have an optical depth of 5 at 2400 Å, was considered to have no distinct absorption at this wavelength. Figure 4 shows, for each of several latitudes on Jupiter, the range of (P_0, τ_a) combinations that give exact fits to the observed intensities at 2400 Å. These curves illustrate the trade-off between the total-absorption optical thickness, τ_a, and the pressure level, P_0, to which the absorbing particles (haze or gas molecules) extend. Thus, for example, the UV brightness of the NPR (at 65° north latitude) requires $\tau_a \geq 3.3$ and $P_0 \leq 40$ mbar. If τ_a = infinity, then P_0 = 40 mbar and we have the model in which there is clean gas above a black surface. If $P_0 = 0$, then $\tau_a = 3.3$ and we have (above 500 mbar) the model in which there is a homogeneously mixed absorber. No more than 340 mbar of clean gas can lie above the GRS—less if we permit τ_a to decrease toward its minimum of 0.4 (for which $\tau_a/\tau_R = 0.24$ above 500 mbar). Analysis of additional data will be necessary in order to select the correct combination of P_0 and τ_a along the line of permitted solutions for a given latitude.

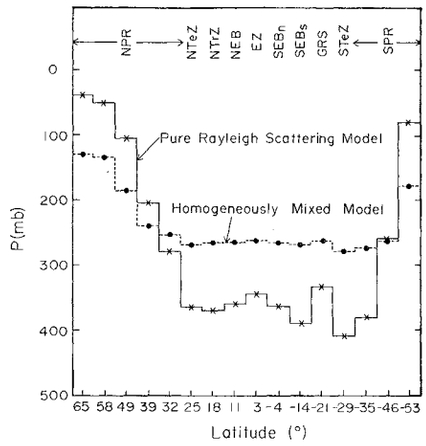

Fig. 3. Effective pressure for absorbing material plotted against latitude in two extreme models. In the pure Rayleigh-scattering model, conservatively scattering gas lies above a black absorbing layer. In the homogeneous model, a semi-infinite optical depth of Rayleigh-scattering gas is mixed with absorbing molecules or particles. In this model, the effective pressure level is for total optical depth equal to unity.

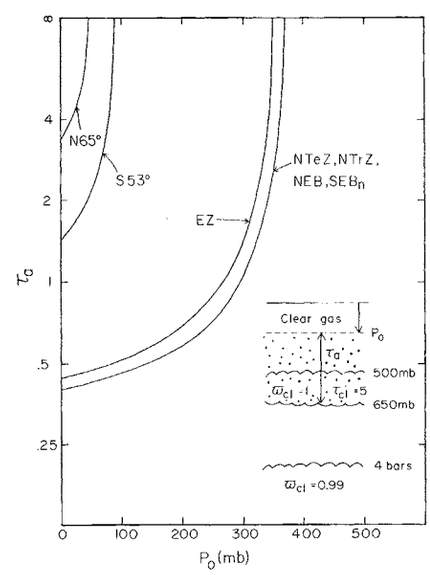

Fig. 4. Relationships between pressure and optical depth for absorbers in the Jovian atmosphere. A schematic diagram of the model used (*5*) is shown at lower right. Permitted combinations of P_0 and τ_a are shown for several latitudes.

It is difficult to determine whether our preliminary analysis of data at 2400 Å is consistent with ground-based (*6*) and spacecraft-based (*3*, *7*) observations at other wavelengths. If the UV absorbers are particulates, we might expect correlation with images of Jupiter in the strong methane band at 8900 Å and in polarization maps. There are some indications that such a correlation exists, particularly at the poles (> 65°) and the equator. However, at latitudes > 30°, the cloud height in our pure Rayleigh-scattering model increases with latitude, in contrast to what is shown by methane-band images and polarization data: deeper clouds at higher latitudes (between about 30° to 50° north and 30° to 60° south). Care must be taken in comparing UV data with data at visible and near-infrared wavelengths because the UV absorbers may not be particulates and, even if they are, their scattering and absorption efficiencies may vary dramatically over a threefold range in wavelength.

Models in which absorbing material high in the atmosphere is generated (as when complex molecules are formed from photochemistry or from electron impact-initiated processes) can account for the extreme absorption in the polar regions. Because of trapping by low temperatures in the Jovian atmosphere, it may be difficult to bring molecular absorbers (those which absorb at 2400 Å) upward to a pressure level of 40 mbar. The absorber could also originate from external precipitation of ionized material, possibly transported from Io or its torus. This material would follow the magnetic field lines and be deposited in the atmosphere in the polar regions. The Jovian rings may be an additional source of material that contributes to absorption in the equatorial zone.

Energetic particle impact leads to the formation of compounds not in thermal equilibrium in the earth's auroral zone. Such processes could have an important effect on the chemistry of Jupiter's upper atmosphere. Several laboratory experi-

ments involving particle bombardment of gas mixtures of methane and hydrogen have demonstrated the production of C_2 to C_5 hydrocarbons in which the saturated aliphatic compound predominates, presumably because of free radical scavenging (*8*). The unique characteristic of this kind of hydrocarbon mixture is that it is colorless in visible light and absorbs substantially in the near UV, especially in the 2000- to 2600-Å range. Assuming that the nitrogen and sulfur compounds, principally NH_3 and H_2S, are trapped by cold at lower altitudes and higher pressures, the radiation and photochemically induced processes should be active high in the atmosphere and should mostly involve CH_4 and H_2.

The Voyager 1 and 2 UV spectrometers detected a very intense auroral ring around the Jovian polar regions that is connected to the Io torus (*9*). Particle precipitation along the magnetic field lines into the Jovian atmosphere provides the mechanism for intense radiation bombardment of the polar region with subsequent radiation-induced chemistry and the production of small-particle UV absorbers at high altitudes. It is interesting to note that the Voyager 1 and 2 infrared interferometer spectrometers (IRIS) have detected marked north-south spatial asymmetry in the ratio of ethane to acetylene, with the saturated hydrocarbon more dominant in the polar domains—indicative, perhaps, of change in equilibrium toward a higher percentage of radiation-induced chemistry (*10*). The IRIS-determined latitudinal dependence appears to follow approximately the asymmetry in latitude of the auroral ring, with the north polar ring extending more southerly to lower latitudes than the south polar ring extends northward (*11*). This may account for the characteristics of the photopolarimeter observations and explain the production of absorbing material at high altitudes.

Further modeling of center-to-limb variations and phase angle variations will permit a much better determination of the altitude distribution and physical characteristics of the absorber.

CHARLES W. HORD
ROBERT A. WEST, KAREN E. SIMMONS
Laboratory for Atmospheric and Space Physics, University of Colorado, Boulder 80309
DAVID L. COFFEEN, MAKIKO SATO
Goddard Institute for Space Studies, 2880 Broadway, New York 10025
ARTHUR L. LANE
JAY T. BERGSTRALH
Jet Propulsion Laboratory, California Institute of Technology, Pasadena 91103

References and Notes

1. C. F. Lillie, C. W. Hord, K. Pang, D. L. Coffeen, J. E. Hansen, *Space Sci. Rev.* **21**, 159 (1977).
2. M. G. Tomasko, in *Jupiter*, T. Gehrels, Ed. (Univ. of Arizona Press, Tucson, 1976), p. 486.
3. A. L. Baker *et al.*, *Science* **188**, 468 (1975); D. L. Coffeen, *J. Geophys. Res.* **79**, 3645 (1974).
4. L. Axel, *Astrophys. J.* **173**, 451 (1972); J. T. Bergstralh, *Icarus* **19**, 390 (1973); R. E. Danielson and M. G. Tomasko, *J. Atmos. Sci.* **26**, 889 (1969); R. A. West, *Icarus* **38**, 34 (1979).
5. M. Sato and J. E. Hansen, *J. Atmos. Sci.* **36**, 1133 (1979).
6. T. Gehrels, B. M. Herman, T. Owen, *Astron. J.* **74**, 190 (1969); D. W. Smith, T. F. Green, R. W. Shorthill, *Icarus* **30**, 697 (1977); R. J. Terrile and J. A. Westphal, *ibid.*, p. 274; W. D. Cochran and D. B. Slavsky, *ibid.* **37**, 84 (1979); R. A. West, *ibid.* **38**, 12 (1979).
7. M. G. Tomasko and S. Martinek, *Bull. Am. Astron. Soc.* **10**, 562 (1978); M. G. Tomasko, R. A. West, N. D. Castillo, *Icarus* **35**, 448 (1978).
8. T. Scattergood and T. Owen, *Icarus* **30**, 780 (1977).
9. A. L. Broadfoot *et al.*, *Science* **204**, 979 (1979); B. R. Sandel *et al.*, *ibid* **206**, 962 (1979).
10. R. Hanel *et al.*, *ibid.*, p. 952.
11. N. S. Ness, M. H. Acuna, R. P. Lepping, K. W. Behannon, L. F. Burlaga, F. M. Neubauer, *Nature (London)* **280**, 799 (1979).
12. We thank the JPL project staff, whose efforts and patience were essential to the success of this experiment. We appreciate the efforts of C. Lillie, P. Theisinger, R. Stahle, R. Morris, R. Hastings, S. Schaffner, C. Barth, I. Stewart, and G. McNutt for their help in making this report a reality. Sponsored by NASA contract 953730 to the Jet Propulsion Laboratory.

26 September 1979

Radio Science with Voyager at Jupiter: Initial Voyager 2 Results and a Voyager 1 Measure of the Io Torus

Abstract. *Voyager 2 radio signals were observed essentially continuously during a grazing occultation of the spacecraft by the southern limb of Jupiter. Intensity data show a classic atmospheric occultation profile and the effects of turbulence and ionospheric focusing and defocusing. No reliable profile of the neutral atmosphere has yet been obtained, primarily because of a combination of large trajectory uncertainties and error multiplication effects associated with the grazing geometry of the Voyager 2 occultation. Analysis of the dispersive ionospheric refraction data yields preliminary profiles for the topside ionosphere at 66.7°S (entry in the evening) and 50.1°S (exit in the morning) that are reversed with respect to corresponding Voyager 1 profiles in terms of plasma concentration at a fixed altitude. Plasma scale heights and temperatures of 880 kilometers, 1200 K and 1040 kilometers, 1600 K were obtained for morning and evening conditions, respectively. Preliminary reduction of the pre-encounter occultation of Voyager 1 by the Io torus yields an average plasma density of about 1000 electrons per cubic centimeter.*

About 22 hours after its closest approach to Jupiter, Voyager 2 passed behind the planet as viewed from the earth. Although the spacecraft was geometrically occulted for nearly 2 hours, the radio links between it and the earth were maintained almost continuously because of the refraction of the signals in Jupiter's south polar atmosphere. Figure 1 shows the plane-of-the-sky geometry of this grazing occultation and preliminary data on the intensity of the spacecraft radio signals as received by the tracking station at Goldstone, California.

The conditions for this occultation differ markedly from the nearly central passage of Voyager 1 behind Jupiter (*1, 2*) and, as a result, somewhat different characteristics of the atmosphere can be studied in the two experiments. In this report, we discuss several general features of the Voyager 2 occultation and present preliminary profiles of the plasma density for the topside of the ionosphere at the two occultation locations. Voyager 1 and 2 were also occulted by the Io torus; we have derived a preliminary result from the Voyager 1 experiment for the density and distribution of plasma in this region. Our previous comments in the Voyager 1 report (*1*) concerning (i) the nature and limitations of the initial data and derived preliminary results and (ii) the need for intensive studies of more complete signal characteristics for all of the potential radio science investigations (*1, 2*) apply to the Voyager 2 data and results as well.

Ionospheric occultation entry of Voyager 2 occurred at about 66.7°S, 254.8°W (system III, 1965.0), and occultation exit was at about 50.1°S, 148.1°W (Fig. 1). Jupiter limb-to-spacecraft distances were about 18 and 19 Jupiter radii (R_J) at entry and exit, respectively, and the maximum angle of refraction in the atmosphere at midoccultation was about 0.3°. This bending would be produced at a pressure level of about 200 mbar in a region about 10 km below the tropopause, under the assumption of an atmospheric structure similar to that measured by Voyager 1 near 12°S latitude (*1*). The intensities and frequencies of the two communications signals (at wavelengths of 3.6 and 13 cm) were measured during the occultation period; only intensity data are shown in Fig. 1 (*3*).

Both atmospheric and ionospheric features are illustrated in the intensity data. At occultation entry (Fig. 1), the ionosphere first caused an increase in the sig-

0036-8075/79/1123-0959$00.50/0 Copyright © 1979 AAAS